Electrical and magnetic properties of AuFe alloys

1999 J. Phys.: Condens. Matter 11 1833

(http://iopscience.iop.org/0953-8984/11/7/013)

J. Phys.: Condens. Matter **11** (1999) 1833–1846. Printed in the UK PII: S0953-8984(99)90706-3

Electrical and magnetic properties of AuFe alloys

Biplab Sanyal†, Parthapratim Biswas†, Tanusri Saha-Dasgupta‡, Abhijit Mookerjee§[+], Ain-ul Huda‖, Nasreen Choudhury‖, Mesbahuddin Ahmed‖* and Amal Halder¶

† S N Bose National Centre for Basic Sciences, JD Block, Sector 3, Salt Lake City, Calcutta 700091, India
‡ Max-Planck-Institut für Festkörperforschung, Stuttgart, Germany
§ Department of Physics, Indian Institute of Technology, Kanpur 208016, India
‖ Department of Physics, University of Dhaka, Dhaka 1000, Bangladesh
¶ Department of Mathematics, University of Dhaka, Dhaka 1000, Bangladesh

Received 14 January 1998, in final form 13 October 1998

Abstract. We study the electronic and magnetic structure of AuFe alloys for varying Fe concentrations. The basis of our study is the augmented-space recursion in conjunction with the local spin-density approximation. We study magnetism from an itinerant-electron viewpoint and show that at low Fe concentrations the random phase arrangement is the more stable phase at $T = 0$ K as compared to the ferromagnetic, antiferromagnetic and paramagnetic arrangements. At higher concentrations the ferromagnetic arrangement becomes the most stable but the average moment decreases with increasing Au concentration.

1. Introduction

AuFe alloys were among the very first alloy systems to be studied because of their interesting behaviour in the low-Fe-concentration regime [1]. The so-called spin-glass phase in these concentration regimes exhibited novel features which made the study of the generic spin-glass transition a topic of considerable interest for decades. Mössbauer studies showed the emergence of the characteristic six-finger pattern at the spin-glass transition temperature T_g, indicating the existence of locally frozen magnetic moments. The dc susceptibility showed a sharp cusp at about the same temperatures, confirming the freezing out of spin degrees of freedom locally. However, there was no indication of long-ranged magnetic ordering or a global magnetic moment. Magnetic relaxation was anomalously slow; there was a large widening and an off-centre shift of the hysteresis curve below the transition. But no response functions showed anomalies around these temperatures. For large Fe concentrations the alloys showed ferromagnetic behaviour of more or less the standard kind. The averaged magnetization decreased with lowering of Fe concentrations, until at around 12–15% of Fe a very complex behaviour sets in which has been described variously in terms of re-entrant spin glasses, randomly canted phases and cluster glasses [3]. This regime then smoothly fits into the spin-glass behaviour below 12% of Fe. The phase diagram is shown in figure 1.

[+] On leave from: S N Bose National Centre for Basic Sciences, Calcutta, India.
E-mail address: abhijit@boson.bose.res.in.
* E-mail address: netproj@bdcom.com.

0953-8984/99/071833+14$19.50

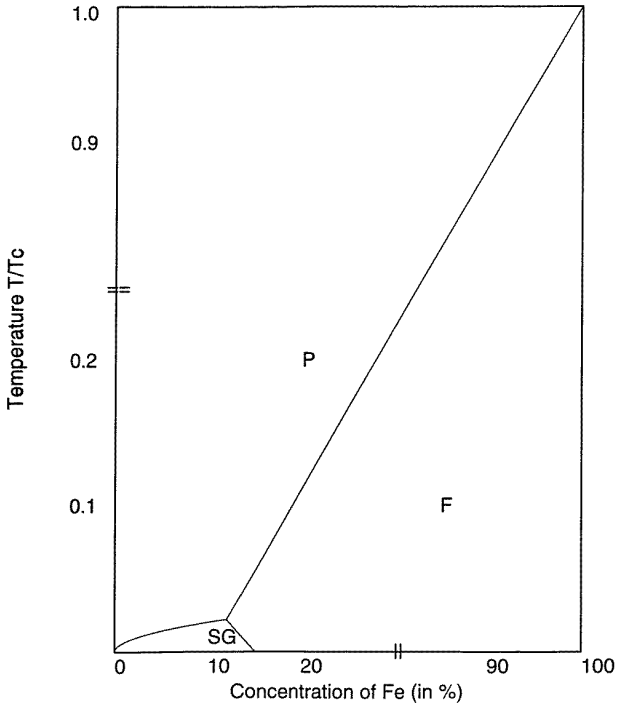

(a)

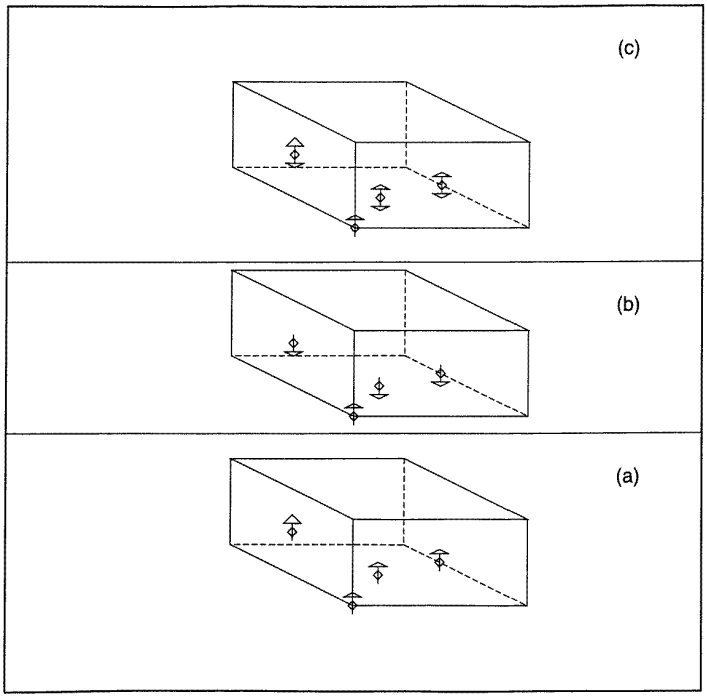

(b)

Figure 1. (a) The magnetic phase diagram for AuFe alloys. (b) A schematic diagram of the different spin arrangements: (a) random ferromagnetic, (b) random antiferromagnetic and (c) random spin arrangements.

Theoretical efforts to understand the nature of these magnetic phases have been extensive. Most approaches, from the simple, down-to-earth rock magnetism ideas to the more sophisticated replica models [2], were invariably based on localized spin statistical models. However, for whole classes of alloys like AuFe and certainly CuMn and a series of ternary stainless steels, the magnetism is most probably of itinerant character. Descriptions of spin glasses from an itinerant-electron viewpoint have been sparse indeed. Muñoz *et al* [4] attempted to provide a first-principles local spin-density approximation (LSDA) picture of AgMn spin-glass alloys within the Korringa–Kohn–Rostoker coherent potential approximation (KKR-CPA). Spin-glass alloys had been studied earlier within the KKR-CPA by Ling *et al* [5]. Recently Ling *et al* [6] also studied AuFe alloys using the KKR-CPA and focused on the origin of short-ranged ordering in these alloys. A complete understanding of the static and dynamic response of these alloys from first principles is still beyond our capability. In this communication we shall attempt to achieve an understanding of the comparative stability of different magnetic arrangements at $T = 0$ K. Ling *et al* [6] have modelled the high-temperature paramagnetic state in terms of the random moment arrangement. We feel that the random moment arrangement of frozen spins is more appropriate in describing the $T = 0$ K state. We shall consider hybridized s and d electrons in Au and Fe as contributing to a Fermi liquid ground state. We shall study the charge and spin densities using the local spin-density approximation (LSDA) and the tight-binding linearized muffin-tin orbital technique (TB-LMTO) within the atomic sphere approximation (ASA) introduced by Andersen and Jepsen [7]. The disorder effect is studied using the augmented-space recursion (ASR) introduced by us earlier [8].

2. Methodology

2.1. The magnetic phases

Description of different magnetic phases within the LSDA involves the evolution of local magnetic moments in the vicinity of ion cores because of the distribution of the valence electron charge. Each lattice site in the face-centred cubic structure is occupied by an ion core: in our case randomly by either Fe or Au. Associated with each ion core is a cell or a sphere, so defined that the charge density contained in the sphere is thought to belong to that ion core alone. Ideally such cells or spheres should not overlap, and this division of space is to a certain extent arbitrary. Within these cells the valence electrons carrying spin σ 'see' a binary random spin-dependent potential $V_\sigma^\nu(\underline{r})$, where $\nu =$ Au or Fe and $\sigma = \uparrow$ or $\downarrow$.

The charge density within the cells can be obtained by solving the Schrödinger equation within the LSDA. The charge density over the solid can be written as

$$\rho_\sigma(\underline{r}) = -(1/\pi)\,\mathrm{Im}\sum_L \int_{-\infty}^{E_\mathrm{F}} \left[x\langle G_{LL}^{\mathrm{Fe},\sigma}(\underline{r},\underline{r},E)\rangle_{\mathrm{av}} + (1-x)\langle G_{LL}^{\mathrm{Au},\sigma}(\underline{r},\underline{r},E)\rangle_{\mathrm{av}}\right] \mathrm{d}E$$

where $\langle G_{LL}^{\mathrm{Fe},\sigma}(\underline{r},\underline{r},E)\rangle_{\mathrm{av}}$ and $\langle G_{LL}^{\mathrm{Au},\sigma}(\underline{r},\underline{r},E)\rangle_{\mathrm{av}}$ are partially averaged Green functions with the lattice site $\underline{r}$ occupied by a Fe or Au ion-core potential corresponding to spin σ. The Au sites are almost spin independent (except for a very small induced moment) and do not appreciably contribute to local moment densities.

For the random ferromagnetic spin arrangement we proceed as follows: we consider all cells to be identical in that they all carry identical average charge densities. We shall borrow the notation of Andersen and Jepsen [7] to write functions like $\tilde{f}(\underline{r}_R)$ which are $f(\underline{r}_R)$ as long as $\underline{r}$ lies in a cell labelled by R and is zero outside. The ferromagnetic charge densities are

defined as

$$\rho_1(\underline{r}) = \sum_R \tilde{\rho}_\uparrow(\underline{r}_R)$$
$$\rho_2(\underline{r}) = \sum_R \tilde{\rho}_\downarrow(\underline{r}_R). \tag{1}$$

The magnetic moment per cell (atom) is then defined by

$$m = (1/N)\int \mathrm{d}^3\underline{r}\ \left[\rho_1(\underline{r}) - \rho_2(\underline{r})\right] = (1/N)\sum_R \int_{r\in R} \mathrm{d}^3\underline{r}\ \left[\tilde{\rho}_\uparrow(r_R) - \tilde{\rho}_\downarrow(r_R)\right]$$
$$= (1/N)\sum_R \int_{r\in R} \mathrm{d}^3\underline{r}\ \tilde{m}(r_R).$$

Since all cells are identical, the above calculation need be done only for one typical cell. Within the TB-LMTO-ASA the cells are replaced by inflated atomic spheres and the remaining interstitial space is neglected. The problem is then one of a binary alloy with an almost non-magnetic charge density due to the Au ion cores and a magnetic one due to the Fe ones.

To describe the antiferromagnetic arrangement, we divide the lattice up into two sublattices $\mathcal{L}$, $\mathcal{L}'$ and redefine the antiferromagnetic charge densities as follows:

$$\rho_1(\underline{r}) = \sum_R \left[\tilde{\rho}_\uparrow(\underline{r}_R)n_R + \tilde{\rho}_\downarrow(\underline{r}_R)(1-n_R)\right]$$
$$\rho_2(\underline{r}) = \sum_R \left[\tilde{\rho}_\downarrow(\underline{r}_R)n_R + \tilde{\rho}_\uparrow(\underline{r}_R)(1-n_R)\right] \tag{2}$$

where n_R takes the value 0 if $R \in \mathcal{L}'$ and 1 if $R \in \mathcal{L}$. If the lattice is nested then it is easy to see that the total magnetic moment per cell (atom) now becomes zero averaged over the entire lattice. However, there are local magnetic moments in each cell which alternate in sign from one sublattice to another. The non-zero staggered magnetic moment per cell is given by

$$m_S = (1/N)\sum_R \int_{r\in R} \mathrm{d}^3\underline{r}\ \tilde{m}(r_R)(1-2n_R).$$

For the paramagnetic arrangement, the charge densities become independent of spin: $\rho_1(\underline{r}) = \rho_2(\underline{r})$. The local moment density itself vanishes. Not only is the globally averaged magnetic moment per cell (atom) zero, but so is the magnetic moment in any cell. This distinguishes the paramagnetic phase from the antiferromagnetic one.

In both of the above cases the problem reduces to that of a binary random alloy between non-magnetic Au atoms and moment-carrying (or non-magnetic in the case of paramagnetic) Fe atoms.

Finally we shall consider the random spin arrangement. Here we shall assume that the cells are randomly occupied by the almost non-magnetic Au ion-core potentials $V^{\mathrm{Au}}(\underline{r})$ with probability $1-x$ and either $V^{\mathrm{Fe}}_\uparrow(\underline{r})$ or $V^{\mathrm{Fe}}_\downarrow(\underline{r})$ with equal probabilities $(x/2)$. The charge densities have expressions identical to those for the antiferromagnetic case:

$$\rho_1(\underline{r}) = \sum_R \left[\tilde{\rho}_\uparrow(\underline{r}_R)n_R + \tilde{\rho}_\downarrow(\underline{r}_R)(1-n_R)\right]$$
$$\rho_2(\underline{r}) = \sum_R \left[\tilde{\rho}_\downarrow(\underline{r}_R)n_R + \tilde{\rho}_\uparrow(\underline{r}_R)(1-n_R)\right]$$

except that the n_R are now *random variables* taking the values 0 and 1 with probabilities 1/2. Since $\langle n_R\rangle_{\mathrm{av}} = 1/2$, it is easy to see that the globally averaged moment density is again zero, but the local magnetic moment, unlike the paramagnetic arrangement, is still non-zero.

If we look at equation (1), it is important to note that although in both the ferromagnetic and the random spin configurations we have partially averaged Green functions, in the former we have a Fe or Au ion core occupying the site $\underline{r}$ immersed in a background of a random binary alloy: Fe-up *or* Fe-down *and* Au, while in the latter an Fe or Au ion occupies the same site but in a background of a ternary random alloy of Fe-up *and* Fe-down *and* Au. The descriptions of randomness in the electronic structures are different in the two cases.

It is also important to note here that the description is basically from an *itinerant viewpoint*. The valence electron cloud which gives rise to the local moments because of a persistent difference between the charge densities ρ_1 and ρ_2 in the ion-core cells is truly delocalized and does not belong to any particular ion core.

2.2. The augmented-space recursion

In earlier communications we have described how to deal with random binary [9] and ternary alloys [10] within the framework of the tight-binding linearized muffin-tin orbital method (TB-LMTO) of Andersen and Jepsen [7] within the augmented-space recursion (ASR). The procedure provides us with a first-principles, self-consistent determination of the configuration-averaged Green function of the disordered alloy. Subsequently we may obtain the density of states, the Fermi energies, the charge and magnetization densities and the total energies of the system. In a series of communications on ordering energies, antiphase boundary energies and phase stabilities of various alloy systems, both non-magnetic and magnetic, we have established the accuracy and usefulness of the TB-LMTO-ASR [8, 9, 13, 15]

Here we need only list the expressions used and refer the reader to the above references for the mathematical details. We shall give the expressions for the ternary alloy alone, since the binary alloy can be thought of as a special case where the concentration of the third component goes to zero. We begin by setting up a muffin-tin potential with centres at the bunch of atomic sites R on a lattice. We inflate the muffin tins into atomic spheres and start from a most-localized TB-LMTO Hamiltonian with random matrix elements:

$$H^{\beta}_{RL,R'L'} = (\tilde{C}_{RL}\delta_{ij}\delta_{LL'})\mathcal{P}_{RL} + (\tilde{\Delta}^{1/2}_{RL}S^{\beta}_{RL,R'L'}\tilde{\Delta}^{1/2}_{R'L'})\mathcal{T}_{RL,R'L'} \tag{3}$$

where $\mathcal{P}$ and $\mathcal{T}$ are projection and transfer operators in the Hilbert space spanned by the minimal tight-binding basis and

$$\tilde{C}_{RL} = C^{\mathrm{B}}_L + \frac{1}{2}(C^{\mathrm{A}}_L - C^{\mathrm{C}}_L)n_R + \frac{1}{2}(C^{\mathrm{A}}_L + C^{\mathrm{C}}_L - 2C^{\mathrm{B}}_L)n^2_R$$
$$\tilde{\Delta}_{RL} = \Delta^{\mathrm{B}}_L + \frac{1}{2}(\Delta^{\mathrm{A}}_L - \Delta^{\mathrm{C}}_L)n_R + \frac{1}{2}(\Delta^{\mathrm{A}}_L + \Delta^{\mathrm{C}}_L - 2\Delta^{\mathrm{B}}_L)n^2_R.$$

Here the potential parameters are labelled with A, B and C which refer to the three constituents of the alloy, and the occupation variables $\{n_i\}$ randomly take the values 1, 0 or -1 according to whether the site labelled by i is occupied by the constituents A, B or C. In a perfectly random alloy the probabilities of such occupations are proportional to the concentrations of the constituents, x_{A}, x_{B} and x_{C}:

$$p(n_R) = x_{\mathrm{A}}\delta(n_R - 1) + x_{\mathrm{B}}\delta(n_R) + x_{\mathrm{C}}\delta(n_R + 1). \tag{4}$$

The augmented-space method now constructs operators $M^{(R)}$ and $N^{(R)}$ corresponding to the variables n_R and n^2_R in the configuration space of rank 3 of each site occupation, $\phi^{(R)}$:

$$M^{(R)} = \sum_{kk'} \Gamma_{kk'}\mathcal{T}^{(R)}_{kk'}$$
$$N^{(R)} = \sum_{kk'} \mathcal{S}_{kk'}\mathcal{T}^{(R)}_{kk'}$$

where $\mathcal{T}^{(R)}_{kk'}$ is the projection operator $\mathcal{P}_{i,k}$ if $k = k'$ and the transfer operator $\mathcal{T}_{i,kk'}$ if $k \neq k'$, both acting on the configuration space $\phi^{(R)}$.

The augmented-space theorem then tells us that the configuration average of the Green function is exactly equal to the following matrix element of the Green function corresponding to the augmented Hamiltonian:

$$\langle G_{RR'}(E)\rangle_{\rm av} = \langle R \otimes \{\emptyset\}\,|(E\tilde{I} - \tilde{H})^{-1}|R' \otimes \{\emptyset\}\rangle \tag{5}$$

where

$$\begin{aligned}\tilde{H} = {} & \sum_{RL} C^{\rm B}_{RL}\mathcal{I}\otimes\mathcal{I} + \sum_{RL,R'L'} h^{\rm BB}_{RL,R'L'}\mathcal{I}\otimes\mathcal{T}_{RL,R'L'} + \sum_{RL}\sum_{k\neq k'} E^{RL}_{kk'}\mathcal{T}^{(R)}_{kk'}\otimes\mathcal{P}_{RL} + \cdots \\ & + \sum_{RL,R'L'}\sum_{kk'}\left\{(h^{\rm BA}_{RL,R'L'}\Gamma_{kk'} + h^{\rm BC}_{RL,R'L'}\mathcal{S}_{kk'})\mathcal{T}^{(R)}_{kk'}\otimes\mathcal{T}_{RL,R'L'}\right\} + \cdots \\ & + \sum_{RL,R'L'}\sum_{kk'}\left\{(h^{\rm AB}_{RL,R'L'}\Gamma_{kk'} + h^{\rm CB}_{RL,R'L'}\mathcal{S}_{kk'})\mathcal{T}^{(R')}_{kk'}\otimes\mathcal{T}_{RL,R'L'}\right\} + \cdots \\ & + \sum_{RL,R'L'}\sum_{k,k'}\sum_{k'',k'''} M^{RL,R'L'}_{k,k',k'',k'''}\mathcal{T}^{(R')}_{k'k''}\otimes\mathcal{T}^{(R)}_{kk'''}\otimes\mathcal{T}_{RL,R'L'}\end{aligned} \tag{6}$$

$E^{RL}_{kk'} = (1/2)(C^{\rm A}_L - C^{\rm C}_L)\Gamma_{kk'} + (1/2)(C^{\rm A}_L + C^{\rm C}_L - 2C^{\rm B}_L)\mathcal{S}_{kk'}$

$M^{RL,R'L'}_{kk'k''k'''} = (h^{\rm AA}_{RL,R'L'} + h^{\rm AC}_{RL,R'L'} + h^{\rm CA}_{RL,R'L'})\Gamma_{k'k''}\mathcal{S}_{k,k'''} + h^{\rm CC}_{RL,R'L'}\mathcal{S}_{k'k''}\mathcal{S}_{kk'''}$

and

$h^{xy}_{RL,R'L'} = (\Delta^x_L)^{1/2}S^{\beta}_{RL,R'L'}(\Delta^y_{L'})^{1/2}$.

The initial TB-LMTO potential parameters are obtained from suitable guessed potentials as described in the article by Andersen and Jepsen [7]. In subsequent iterations the potential parameters are obtained from the solution of the Kohn–Sham equation

$$\left\{-\frac{\hbar^2}{2m}\nabla^2 + V^{\nu\sigma} - E\right\}\phi^{\nu}_{\sigma}(r_R, E) = 0 \tag{7}$$

where

$$V^{\nu\sigma}(r_R) = V^{\nu\sigma}_{\rm core}(r_R) + V^{\nu\sigma}_{\rm Har}(r_R) + V^{\nu\sigma}_{\rm xc}(r_R) + V_{\rm Mad}. \tag{8}$$

Here ν refers to the species of atom sitting at R and σ the spin component. The electronic position within the atomic sphere centred at R is given by $r_R = r - R$. The core potentials are obtained from atomic calculations and are available for most atoms.

The Hartree potential needs discussion. Let us denote the atomic sphere centred at R by S_R. If we wish to obtain the Hartree potential within the atomic sphere S_R when an atom of the type ν sits at R, the configuration space at the site R is projected onto the fixed configuration ν, while the configuration at the remaining sites is, say, random binary. Let us denote the 'average state' by $\{\nu \in R \otimes \emptyset\}$ (the reader is referred to Saha *et al* [8] for the details of the configuration notation and the basic augmented-space theorem); then,

$$\begin{aligned}V^{\nu\uparrow}_{\rm Har}(r_R) = {} & e^2\int_{S_R} {\rm d}^3r'_R\,\frac{\rho^{\nu}_{\uparrow}(r'_R)}{|r_R - r'_R|}\cdots + e^2\sum_{R''\neq R}\int_{S_{R''}}{\rm d}^3r'_{R''}\,\frac{\langle\rho(r'_{R''})\rangle}{|r_R - r'_{R''}|}\cdots \\ & + e^2\sum_{R''\neq R}\int_{S_{R''}}{\rm d}^3r'_{R''}\,\frac{\delta\rho(r'_{R''})}{|r_R - r'_{R''}|}\end{aligned}$$

where

$$\begin{aligned}\delta\rho(r'_{R''}) = {} & \frac{-1}{\pi}\,{\rm Im}\int_{-\infty}^{E_{\rm F}}{\rm d}E\,\big[\langle\{r'_{R''}\otimes A\in R''\otimes\emptyset\}|\tilde{G}(E)\otimes\tilde{M}_{R''}|\{r'_{R''}\otimes A\in R''\otimes\emptyset\}\rangle\cdots \\ & \cdots - \langle\{r'_{R''}\otimes B\in R''\otimes\emptyset\}|\tilde{G}(E)\otimes\tilde{M}_{R''}|\{r'_{R''}\otimes B\in R''\otimes\emptyset\}\rangle\big].\end{aligned}$$

$\tilde{G}(E)$ is the augmented-space resolvent $(z\tilde{I}-\tilde{H})^{-1}$ and $\tilde{M}_{R''}$ is the configuration operator, e.g. for the binary randomness $\tilde{M}_{R''} = I \otimes \cdots \otimes M_{R''} \otimes I \otimes \cdots$ and, if x is the concentration of the A component,

$$M_{R''} = \begin{pmatrix} 0 & \sqrt{x(1-x)} \\ \sqrt{x(1-x)} & 1-x \end{pmatrix}.$$

The first two terms are identical to the usual expressions for the CPA [6]. Of course, the partially averaged and averaged charge densities in the ASR have the effects of configuration fluctuation of the immediate environment of the atomic site associated with the atomic sphere included. The last term represents configuration fluctuations in the charge densities associated with atomic spheres other than S_R. This correction is taken only up to the nearest-neighbour environment of S_R.

The exchange–correlation potential is a functional of the charge and magnetic moment densities $\rho^{\nu\uparrow}(r_R)$, $\rho^{\nu\downarrow}(r_R)$, $m^{\nu\uparrow}(r_R)$ and $m^{\nu\downarrow}(r_R)$. We have used the von Barth–Hedin form of the exchange functional. For a random alloy the Madelung potential is difficult to define as it depends upon the distant environment in a given configuration. We choose our atomic sphere radii of the components in such a way that they preserve the total volume on average and individual atomic spheres are neutral. The effective Madelung term then vanishes.

As in the CPA calculations, we iterate until the total energy and moments of the charge density converge. In this sense our calculations are self-consistent in the LSDA sense.

In spite of several publications describing it in detail, it seems that there still remains confusion over what the TB-LMTO-ASR actually achieves. It may be relevant to comment on this in brief here. The ASR obtains averaged quantities like $\langle G^{\sigma}_{LL}(\underline{r}, \underline{r}, E)\rangle_{\mathrm{av}}$ and partially averaged quantities like $\langle G^{\nu\sigma}_{LL}(\underline{r}, \underline{r}, E)\rangle_{\nu\sigma}$ via recursion in the full augmented space. Whereas in the coherent potential approximation (CPA) the entire environment of an atom is replaced by an effective medium, the ASR includes the effect of the immediate environment. If the disorder is homogeneous, it has been shown [11] that there exists a corresponding translation symmetry in augmented space which ensures that the effects of the environment on each atom are identical. In a recent communication we have demonstrated the convergence of integrals involving the averaged density of states with the number of exact recursion steps and termination [12], and have shown that given a preassigned allowable error window, the recursion can be tailored such that the error in the integrals remains within the window. In a series of communications on ordering energies, antiphase boundary energies and phase stabilities of various alloy systems, both non-magnetic and magnetic, we have established the accuracy and usefulness of the TB-LMTO-ASR [8, 9, 13–15]

2.3. Computational details

For the calculation of the component-projected averaged density of states of the binary and ternary models related to the four different magnetic arrangements, we have used a real-space cluster of 400 atoms and an augmented-space shell up to the sixth-nearest neighbour from the starting state. Eight pairs of recursion coefficients were determined exactly and the continued fraction terminated by the analytic terminator due to Luchini and Nex. In a recent paper, Ghosh *et al* [12] have discussed the convergence of various integrated quantities, like the Fermi and the band energies, within the augmented-space recursion. The convergence tests suggested by the authors were carried out to prescribed accuracies. We have reduced the computational burden of the recursion in the full augmented space by using the local symmetries of the augmented space to reduce the effective rank of the invariant subspace in which the recursion is confined [9] and using the seed recursion methodology with fifteen energy seed points uniformly across the

spectrum. Both the reduction techniques have been described in detail in the references and readers are referred to them for details. It is important to emphasize this point, since there have been erroneous statements made earlier that although the augmented-space recursion method is attractive mathematically, it was not feasible for application as a computational technique to realistic alloys. Furthermore, it has been shown [9] that augmented-space recursion with an analytic terminator *always* produces herglotz results, whether we use the homogeneous disorder model as in this paper or the version including short-ranged order [16] or local lattice distortions [17].

We have chosen the Wigner–Seitz radii of the two constituent atoms Fe and Au in such a way that the average volume occupied by the atoms is conserved. Within this constraint we have varied the radii such that the final configuration has neutral spheres. This provides the simplest way of eliminating the necessity of including the averaged Madelung energy part in the total energy of the alloy. The definition and computation of the Madelung energy in a random alloy had faced controversy in recent literature [18] and to this date no really satisfactory resolution of the problem exists. Simultaneously we have made sure that the sphere overlap remains within the 15% limit prescribed by Andersen.

The calculations have been made self-consistent in the LSDA sense; that is, at each stage the charge densities are calculated from the augmented-space recursion and the new potential is generated by the usual LSDA techniques. This self-consistency cycle was converged in both total energy and charge to errors of the order of 10^{-5}. We have also minimized the total energy with respect to the lattice constant. The quoted results are those for the minimum-energy configuration. No short-ranged order due to chemical clustering has been taken into account in these calculations, nor any lattice distortions due to the size differences between the two constituents.

3. Results

Figure 1(a) gives us an idea of the magnetic phase diagram for AuFe. Note that up to the lowest Au concentrations the alloys are all face-centred cubic. The phase digram has been culled out of experimental data.

Figure 1(b) shows a schematic description of (a) the random ferromagnetic, (b) the random antiferromagnetic and (c) the spin-disordered arrangements on a fcc lattice.

Magnetic moments are very sensitive to the lattice spacing. This is particularly true for itinerant magnets. The Stoner criterion clearly shows that magnetic moment is dependent on the effective d-band widths, which in turn depend upon the lattice spacing. We have minimized the total energy as a function of the lattice parameter a and reported results for the minimum configuration. In figure 2 we show the total energy versus the lattice parameter for the alloy with 90% Fe. The minimum occurs at $a \simeq 3.625$ Å which is slightly less than the Vegard's law value of 3.64 Å. This is expected, since the LSDA overestimates bonding, and usually predicts a lower lattice parameter for the lowest-energy configuration and therefore, by the Stoner criterion, a lower magnetic moment.

In figures 3(a) and 3(b) we show the density of states for the ferromagnetic AuFe alloys for concentrations of (a) 2.5% and (b) 90% of Fe. For case (a), the host Au partial density of states resembles that for pure Au, with little exchange splitting. The impurity Fe partial densities of states show very little structure, but are exchange split, giving rise to local moments on the Fe atoms. For case (b), the host Fe partial densities of states show exchange splitting and structure, while the impurity Au partial densities of states have little structure. They however show a small exchange splitting, indicating a small induced moment on the Au atoms.

Figure 3(c) shows the density of states for a concentration of 25% of Fe. Ling *et al* [6]

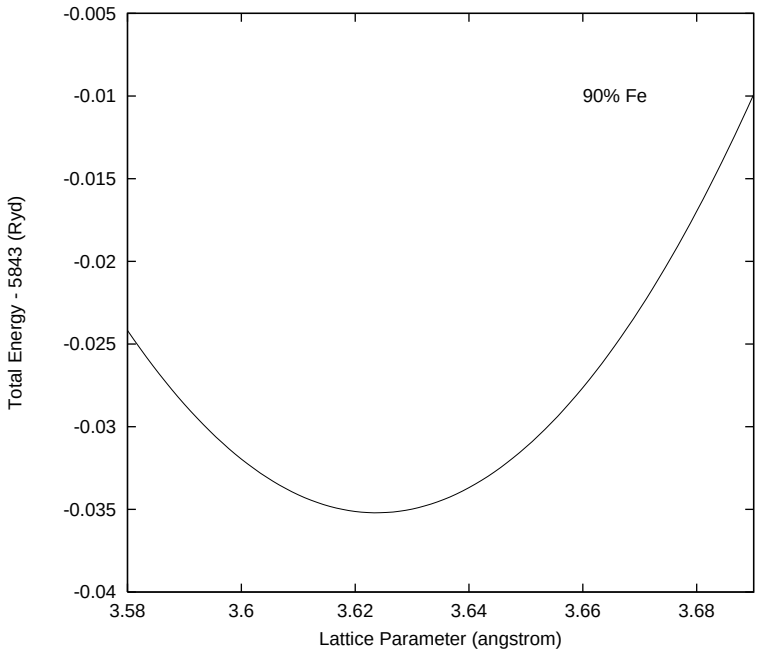

Figure 2. Total energy versus the lattice parameter for the alloy with 90% Fe.

have also studied the same alloy using the KKR-CPA. Comparison with their results shows that for both the majority and minority bands the KKR-CPA overlaps between Au and Fe partial densities of states are larger than those shown in our results. In fact, the majority Au and Fe bands in the KKR-CPA have almost identical band centres, a feature which does not show up in the TB-LMTO-CPA calculations either.

Figure 3(d) shows the density of states for the 10% Fe alloy in the random moment configuration. The Fe partial density of states is locally exchange split and that for Au shows considerable structure. Again the results are similar to the KKR-CPA work of Ling *et al* [6] with slightly smaller overlap between the Au and the Fe densities of states.

For the high Fe concentrations the Au atom carries almost no magnetic moment, while the $Fe_{\uparrow}$ and the $Fe_{\downarrow}$ states are exchange split in energy, giving rise to a local magnetic moment.

In figure 4 we plot the total-energy differences between the random-moment phase and the ferromagnet: $E_{\text{random}} - E_{\text{ferro}}$. The antiferromagnetic and the paramagnetic arrangements have higher energies across the entire concentration regime, and so are not mentioned in the figure. In the high-concentration regime, the difference is positive. This means that the ferromagnetic arrangement is the more stable. Around 10%—in fact at concentrations very slightly below this—the energy difference changes sign. In other words, in these low-magnetic-concentration regimes, the random spin configuration appears to be the stable phase.

In figure 5 we plot the local and averaged magnetic moments as functions of the Fe concentration. The local moment on Au is small throughout the concentration range, but is larger for larger Fe concentrations. This is expected from the larger exchange splitting in the Au partial densities of states for higher Fe concentrations as shown earlier. The local moment on Fe increases as the concentration of Au increases. In the concentrated Fe regime, where the overlap between Fe atoms is large and the Fe partial densities of states are wider, the local moment is around 2.2 μ_B/atom. As the concentration of Au increases, the Fe partial densities

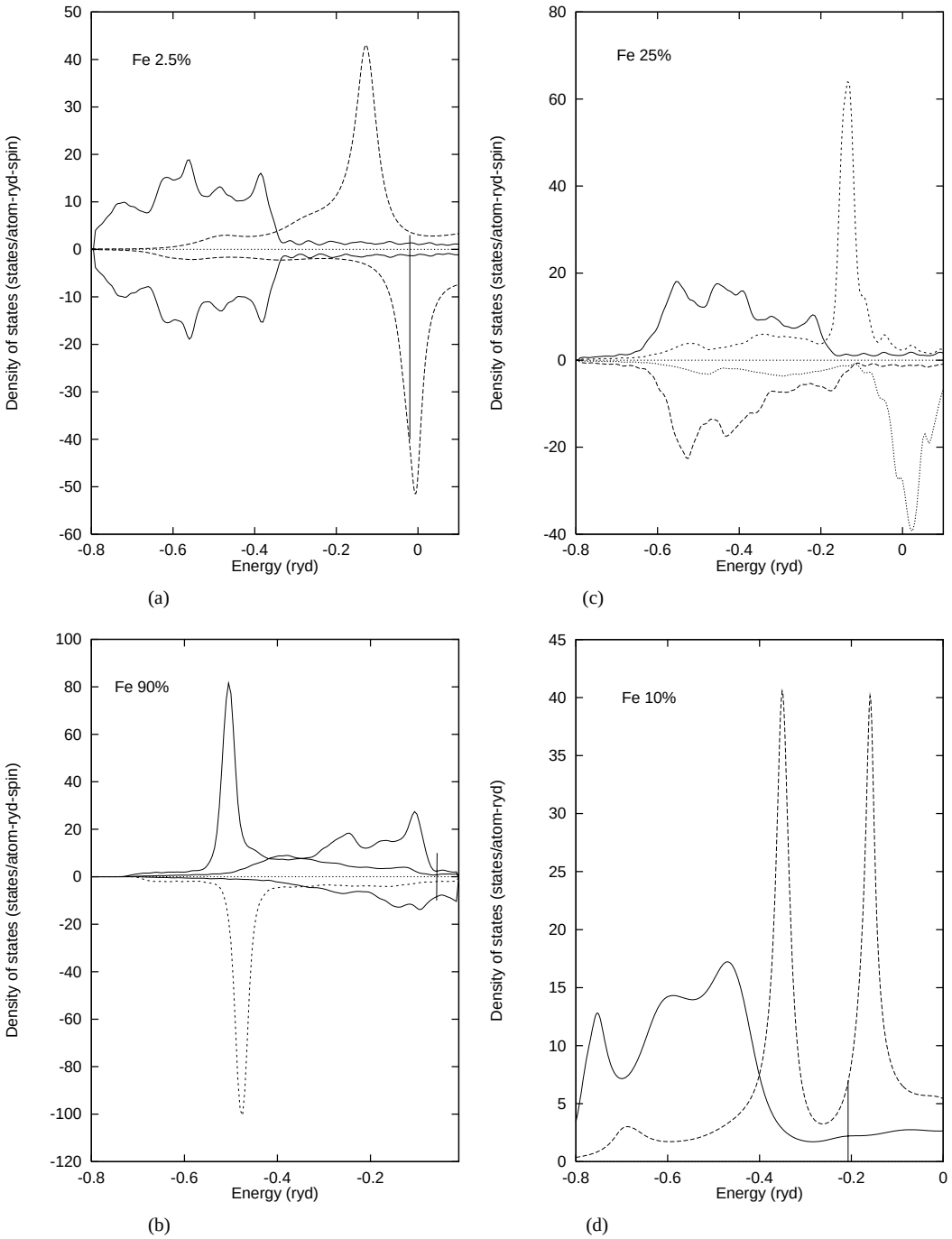

Figure 3. The partial density of states on the Au and Fe atoms in ferromagnetic AuFe alloys at the following Fe concentrations: (a) 2.5%, (b) 90% and (c) 25%; and in the random-moment AuFe alloy at an Fe concentration of (d) 10%. The Fermi energies are shown as dashed curves.

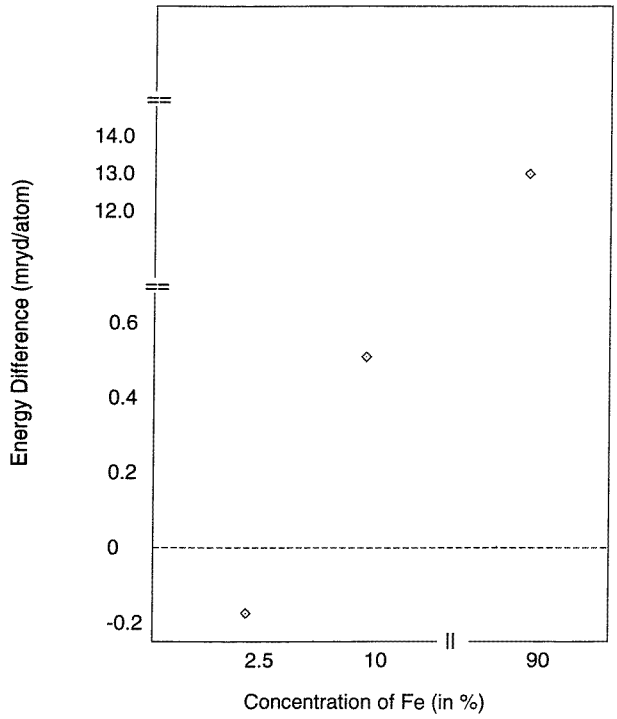

Figure 4. The difference between the total energies of the random and ferromagnetic phases as a function of the concentration.

of states become narrower. The Stoner criterion would suggest a higher moment, which is indeed observed. The local moment on Fe in the impurity regime is about 3.4 μ_B/atom. We should compare this with the moment on free Fe atoms, which is about 4 μ_B. This simple argument carries through particularly, since the overlap between the Fe and Au d bands is rather small. A rather similar increase in local moment is also seen when the Fe d densities of states become narrower when bcc Fe overlayers form on fcc Ag substrates [19].

The average moment decreases steadily, initially linearly, as the concentration of Fe decreases. At the transition to the random-spin phase, this drops steeply to zero and remains so in this new phase. This behaviour is supported by experimental data on the alloy. The concentration regime around 14%–10% is bedevilled with possible mixed phases, micto-magnetic phases and cluster glass phases, all of which require short-ranged magnetic ordering. Since short-ranged and clustering effects are absent in our work, we cannot hope to reproduce such 'dirty' behaviour.

A note on a rather unsatisfactory feature of the results quoted above: near the concentration at which the random spin arrangement 'wins' over the ferromagnetic one, the energy differences are at the very limit of accuracy of the LMTO-ASA method itself. However, the trend of the energy difference decreasing with decreasing concentration of Fe and finally changing sign is what we emphasize, rather than the actual energy difference values themselves.

Finally, for the 90–10 alloy we have carried out the augmented-space recursion in k-space [20] to obtain the spectral functions and hence the complex bands. This is shown in figure 6. The d bands of Au and Fe are well separated—this is a case of a split-band alloy. The e_g–t_{2g} bands of Au are clearly seen beginning at -0.6 and -0.5 Ryd at the Γ point and flaring

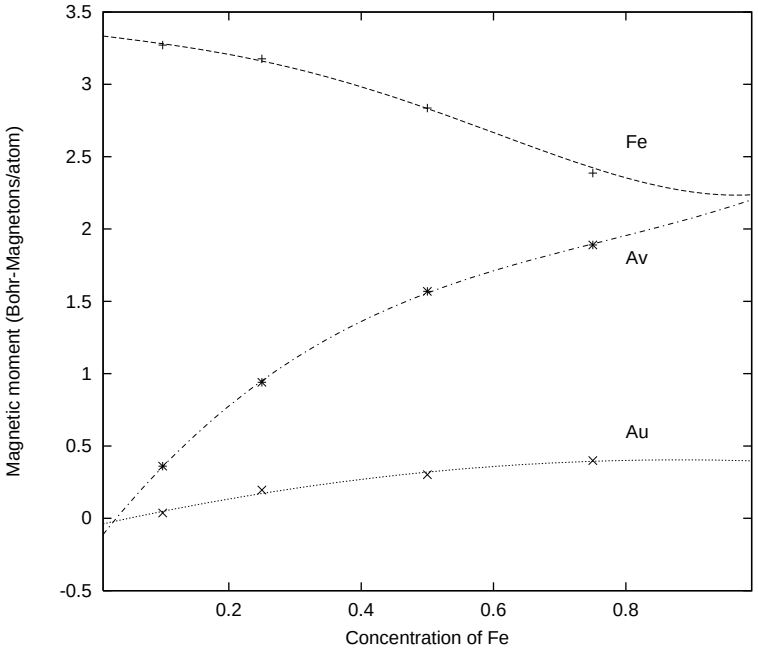

Figure 5. The variation of the local magnetic moment per atom in the ferromagnetic phase as a function of concentration.

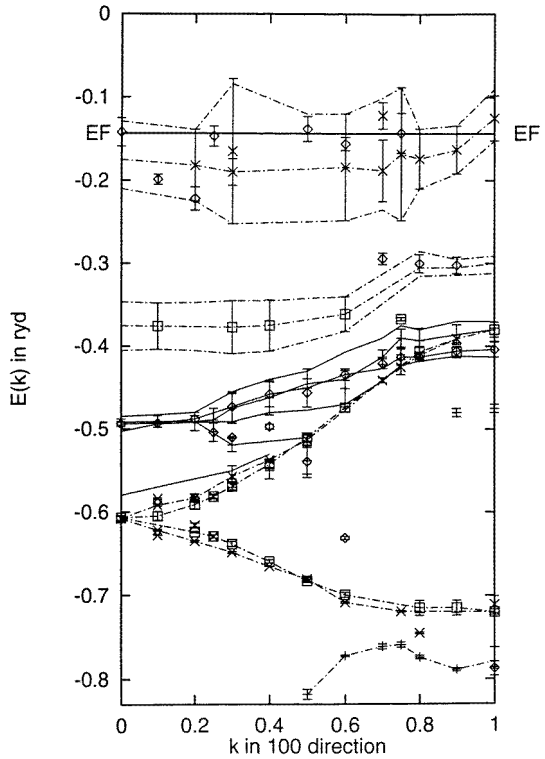

Figure 6. The complex bands for the 90–10 AuFe alloy obtained from augmented-space recursion in *k*-space.

out to a width of around 0.35 Ryd at the X point. Below these bands we see the top of the hybridized s band dropping below −0.8 Ryd. These *host* bands of Au are not characterized by large lifetimes. Most of the width arises from hybridization rather than disorder scattering. The up and down bands of Fe show up clearly, starting at −0.35 Ryd and −0.15 Ryd at the Γ point. These impurity bands are narrow (as is characteristic of impurity bands) and the lifetimes associated with their widths (particularly in the minority band) are large. We expect impurity bands to show the maximum effect of disorder scattering. It is known that because of strong-disorder scattering, the coherent potential approximation does not work well in impurity bands. The Fermi energy cuts the minority band just above half its width. The lifetimes of the bands crossing the Fermi surface are large and we expect the Fermi surface to be very fuzzy in these alloys.

We must comment on one more aspect of a true spin-glass phase which is not reflected in our work. We have chosen a global quantization axis with respect to which we describe the spin configurations as ↑ and ↓. The random spin arrangement that we have described here is with respect to such a picture. In a spin-glass phase, we expect there to be a local quantization axis which randomly varies from site to site. Description of such locally varying quantization axes will require a generalization of the LSDA approach itself. There have been several attempts to describe 'non-collinear' magnetism. Gyorffy *et al* [21] and Sandratskii and Kübler [22] have carried out extensive work on non-collinear magnetism. The review by Sandratskii [23] gives an extensive account of the approach. Lorenz and Hafner [24] and Spišak and Hafner [25] have also given a beautiful description of how to deal with such random arrangements of spins. Our intuitive idea of what the spin arrangement in a spin glass should be is much nearer to such a description. We propose to use these ideas in a subsequent communication.

Acknowledgments

We should like to thank the International Centre for Theoretical Physics, Trieste, for financial help through its Network programme. One of us (PB) would like to thank the CSIR, India, for financial assistance. AM would like to thank the IIT, Kanpur, for hospitality during his sabbatical leave.

References

[1] Mydosh J 1978 *J. Magn. Magn. Mater.* **7** 237
[2] Chowdhury D and Mookerjee A 1984 *Phys. Rep.* **114** 1
Wohlfarth E P 1977 *Physica* A **86–88** 852
Parisi G 1980 *J. Phys. A: Math. Gen.* **13** L115
Parisi G 1980 *J. Phys. A: Math. Gen.* **13** 1101
Parisi G 1980 *J. Phys. A: Math. Gen.* **13** 1887
Parisi G 1979 *Phys. Rev. Lett.* **43** 1754
[3] Mookerjee A 1979 *Pramana* **14** 11
Villain J 1979 *Z. Phys.* B **33** 31
Gabay M and Toulouse G 1981 *Phys. Rev. Lett.* **47** 201
Hamzic A and Campbell I A 1981 *J. Physique* **42** L309
Nigam A K, Girish Chandra and Ramakrishnan S 1986 *J. Phys. F: Met. Phys.* **16** 1255
[4] Muñoz M C, Gyorffy B L and Verhuyck K 1983 *J. Phys. F: Met. Phys.* **13** 1847
[5] Ling M F, Staunton J B, Johnson D D and Pinski F J 1994 *Europhys. Lett.* **25** 631
[6] Ling M F, Staunton J B, Johnson D D and Pinski F J 1995 *Phys. Rev.* B **52** 3816
[7] Andersen O K and Jepsen O 1984 *Phys. Rev. Lett.* **53** 2571
[8] Saha T, Dasgupta I and Mookerjee A 1994 *J. Phys.: Condens. Matter* **6** L245
[9] Dasgupta I, Saha T and Mookerjee A 1996 *J. Phys.: Condens. Matter* **8** 1979
[10] Saha T and Mookerjee A 1997 *J. Phys.: Condens. Matter* **9** 6607

[11] Biswas P, Sanyal B, Mookerjee A, Huda A, Halder A and Ahmed M 1997 *Int. J. Mod. Phys.* B **11** 3715
[12] Ghosh S, Das N and Mookerjee A 1997 *J. Phys.: Condens. Matter* **9** 10 701
[13] Dasgupta I, Saha-Dasgupta T, Mookerjee A and Das G P 1997 *J. Phys.: Condens. Matter* **9** 3259
[14] Saha T and Mookerjee A 1997 *J. Phys.: Condens. Matter* **9** 2179
[15] Sanyal B and Mookerjee A, 1998 *Phys. Lett.* A **10**
[16] Mookerjee A and Prasad R 1993 *Phys. Rev.* B **48** 17 724
Dasgupta I, Saha T and Mookerjee A 1993 *Phys. Rev.* B **51** 17 724
[17] Saha T, Dasgupta I and Mookerjee A 1995 *J. Phys.: Condens. Matter* **7** 3413
[18] Gonis T and Kudrnovský J 1997 *J. Phys.: Condens. Matter* **9**
[19] Sanyal B, Biswas P P, Mookerjee A, Salunke H, Das G P and Bhattacharyya A K 1998 *J. Phys.: Condens. Matter* **10** 5767
[20] Sanyal B, Biswas P P, Fakhruddin M, Halder A, Ahmed M and Mookerjee A 1995 *J. Phys.: Condens. Matter* **7** 8569
[21] Gyorffy B L, Pindor A J, Staunton J, Stocks G M and Winter H 1982 *J. Phys. F: Met. Phys.* **12** 177
[22] Sandratskii L M and Kübler J 1992 *J. Phys.: Condens. Matter* **4** 6927
Sandratskii L M and Kübler J 1996 *Europhys. Lett.* **33** 447
Sandratskii L M and Kübler J 1996 *Phys. Rev. Lett.* **76** 4963
[23] Sandratskii L M 1998 *Adv. Phys.* **47** 91
[24] Lorenz R and Hafner J 1995 *J. Magn. Magn. Mater.* **139** 209
[25] Spišak D and Hafner J 1997 *Phys. Rev.* B **55** 8304